Spectral dynamics in the B800 band of LH2 from Rhodospirillum molischianum: a single molecule study

Hofmann, C.; Aartsma, T.J.; Michel, H.; Köhler, J.

Spectral dynamics in the B800 band of LH2 from *Rhodospirillum molischianum*: a single-molecule study

2004 New J. Phys. 6 8

(http://iopscience.iop.org/1367-2630/6/1/008)

New Journal of Physics
An Institute of Physics and Deutsche Physikalische Gesellschaft Journal

Spectral dynamics in the B800 band of LH2 from *Rhodospirillum molischianum*: a single-molecule study

Clemens Hofmann[1], **Thijs J Aartsma**[2], **Hartmut Michel**[3] **and Jürgen Köhler**[1,4]

[1] Experimental Physics IV and BIMF, University of Bayreuth, 95440 Bayreuth, Germany
[2] Department of Biophysics, Huygens Laboratory, Leiden University, P.O. Box 9504, 2300 RA Leiden, The Netherlands
[3] Department of Molecular Membrane Biology, Max-Planck Institute of Biophysics, 60439 Frankfurt, Germany
E-mail: juergen.koehler@uni-bayreuth.de

New Journal of Physics **6** (2004) 8
Received 14 October 2003
Published 30 January 2004
Online at http://www.njp.org/ (DOI: 10.1088/1367-2630/6/1/008)

Abstract. The BChl *a* absorptions in the B800 spectrum of individual LH2 complexes from *Rhodospirillum molischianum* show sudden, reversible spectral jumps between a finite number of spectral positions. From our data, we conclude that these fluctuations result from conformational changes of the protein backbone in close vicinity of the chromophores which provides a sensitive tool to monitor local modulations of the pigment–protein interaction.

Contents

[4] Author to whom any correspondence should be addressed.

PII: S1367-2630(04)70350-X

1. Introduction

Since the beginning of single-molecule spectroscopy in the late 1980s [1, 2], the field has undergone breathtaking progress; in particular, the application of single-molecule detection techniques to biology and biochemistry has led to a revolution in these disciplines. Fascinating experiments became possible, such as the stretching and twisting of DNA [3], the use of autofluorescent proteins to monitor processes in living cells [4], the observation of an optomechanical cycle on a single molecule [5], the quest for sequencing single DNA molecules [6], the registration of the movement of an individual myosin head along an actin filament upon hydrolysis of a single ATP [7] or monitoring molecular rotations upon F1-ATPase [8].

The intriguing feature of this technique is that it allows us to elucidate information that is commonly washed out by ensemble averaging. Besides the possibility to circumvent spatial inhomogeneities, it allows also the observation of dynamical processes that are usually obscured by the lack of synchronization within an ensemble. A single molecule that undergoes a temporal development between different states is at any time in a distinct, well-defined state and the whole sequence of steps can be studied. This allows in particular the identification of short-lived intermediate states that might be essential for the understanding of the process under study but which would be completely masked otherwise.

In most of such experiments, an individual chromophore is linked to the object of interest, for instance a protein or a piece of DNA, and is detected via its laser-induced fluorescence. Basic requirements that have to be fulfilled by a chromophore suited for single-molecule spectroscopy are photophysical and photochemical stability and a high fluorescence quantum yield. As long as the emission can be discriminated from the unavoidable background, the chromophore provides a digital signal: 'present' or 'not present' which allows us to extract valuable information about the substrate, for instance its mobility, its spatial position or its status of activity.

By the overwhelming success of single-molecule detection in the life sciences, the centre of gravity of the field has shifted away from its cryogenic roots [1, 2]. However, the low-temperature approach allows to study single molecules over a very long observation period because photobleaching effects of the probe molecules, usually limiting the observation time to some tens of seconds under ambient conditions, are negligible. This offers the opportunity to determine the electronic eigenstates of an individual system, i.e. to perform single-molecule *spectroscopy* rather than single-molecule *detection* and to apply many experimental techniques from the highly developed toolbox of spectroscopy also to single objects [9]–[14].

In this paper, we report about the spectroscopy of individual pigment–protein complexes from a purple bacterium—*Rhodospirillum molischianum*. These bacteria absorb sunlight by a network of antenna pigment proteins and transfer the excitation energy efficiently to the photochemical reaction centre (RC), where a charge separation takes place, providing the free energy for subsequent chemical reactions. It is known that most of these bacteria contain two types of antenna complexes: light-harvesting complex 1 (LH1) that is closely associated with the RC and light-harvesting complex 2 (LH2). The progress made in high-resolution structural studies of light-harvesting complexes of purple bacteria [15]–[17] has strongly stimulated experimental and theoretical investigations to understand the efficient energy transfer in these antenna systems. The x-ray structure of the LH2 complex [15, 16] shows a remarkable symmetry in the arrangement of the light-absorbing pigments in their protein matrix. The basic building block of LH2 is a protein heterodimer ($\alpha\beta$), which binds three BChl *a* pigments and one carotenoid molecule. The LH2 complex consists either of nine (*Rhodopseudomonas acidophila*,

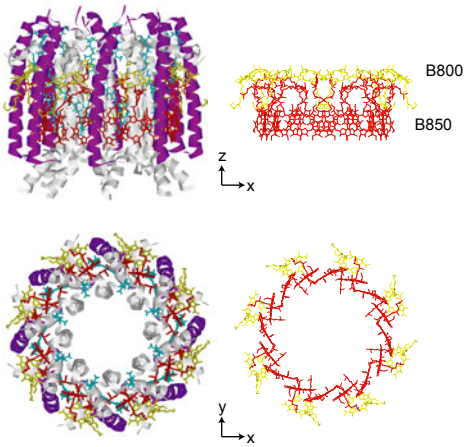

Figure 1. X-ray structure of the LH2 complex from *Rs. molischianum* [16]. Left panel: the pigment–protein complex is displayed as a whole; right panel: only the BChl *a* molecules are shown for clarity. The upper panel of the figure shows a side view, the lower part of the figure shows a top view of the structure. The BChl *a* molecules are arranged in two concentric rings commonly termed B800 (yellow) and B850 (red) ring. The atomic co-ordinates were taken from the Protein Data Bank, identification code 1LGH.

Rhodobacter sphaeroides) or eight (*Rhodospirillum molischianum*) such $\alpha\beta$-polypeptide heterodimers. In figure 1, we show the structure of the LH2 complex from *Rs. molischianum* which has been obtained by x-ray crystallography with an resolution of 2.4 Å [8]. (The x-ray structure from LH2 of *Rhodopseudomonas acidophila* as well as that of the reaction centre from *Rhodobacter sphaeroides* can be found at http:// www.gla.ac.uk/ibls/BMB/rjc/resint.htm.) In the multimedia enhancement accompanying this paper, an interactive three-dimensional (3D) representation of the complex is provided. The left panel of figure 1 shows the pigment–protein complex as a whole, the right panel shows only the BChl *a* molecules for clarity. For *Rs. molischianum*, the LH2 complex is an octameric hollow cylinder that comprises 24 BChl *a* molecules arranged in two concentric rings. One ring consists of a group of eight well-separated BChl *a* molecules (B800) absorbing light at about 800 nm (12 500 cm^{-1}). The other ring consists of 16 closely interacting BChl *a* molecules (B850), which absorb at about 850 nm (11 765 cm^{-1}). Energy transfer within the LH2 complex occurs from the B800 to the B850 molecules in less than 1 ps, whereas among the B850 molecules it is an order of magnitude faster. The transfer of energy from LH2 to LH1 and, subsequently, to the reaction centre occurs *in vivo* on a time scale of 5–10 ps, i.e. very fast compared to the decay of an isolated LH2 which has a fluorescence lifetime of 1.1 ns.

By now, it has been established that the spatial structure of photosynthetic complexes, especially the mutual orientation of the pigments, determine to a large extent their spectroscopic features and excited-state dynamics [18]. Important parameters that determine the character of the electronically excited states are the strength of the intermolecular interaction V and the spread in-site energy Δ of the individual pigments (diagonal disorder). For the B850 system, the ratio V/Δ is sufficiently large that a description of the excited states in terms of delocalized Frenkel excitons is appropriate [19, 20]. For the B800 molecules, the interaction

strength is about one order of magnitude smaller with respect to the B850 molecules, and the coupling between these molecules is in the weak to intermediate regime [21]. In first approximation, the excitations can be treated as being localized on an individual BChl *a* molecule.

Generally, information about the parameters that determine the description of the electronic structure of light-harvesting complexes can be obtained by optical spectroscopy. But even isolated protein–pigment complexes of photosynthetic systems are rather complex, and it has been proven difficult to analyse the excited-state properties of these systems in all details. This is mainly caused by the pronounced disorder in these types of systems, which masks details in the steady-state optical spectra, even at low temperature. We have investigated light-harvesting complexes from purple bacteria by applying single-molecule spectroscopic techniques. The results of these studies have been documented in a series of publications [19]–[27]. Here, we present a study on the B800 band of LH2 from *Rs. molischianum*, where we investigate the details of the interaction of the B800 pigments with the protein backbone. Owing to the relative weak intermolecular interaction between the B800 BChl *a* molecules, these are suited to act as reporters of their local environment providing information about conformational changes of the protein scaffold.

2. Experimental

LH2 complexes from *Rs. molischianum* were isolated and purified as described previously [28], and the resulting solution was diluted in several steps to a concentration of about 1×10^{-11} M. Dilution was performed in detergent buffer to prevent the complexes from aggregation or dissociation; in the last step, also 1.8% (w/w) polyvinyl alcohol (PVA; $M_w = 125\,000\,\mathrm{g\,mol^{-1}}$) was present. A drop (10 μl) of this solution was spin-coated on a lithium fluoride (LiF) substrate by spinning it for 15 s at 500 rpm and 60 s at 2000 rpm, producing high-quality amorphous polymer films with a thickness of less than 1 μm in which the pigment–protein complexes are embedded. LiF was chosen as substrate because the inversion symmetry of the alkali halide crystal prevents first-order Raman scattering and the optical resonances are far in the UV. The samples were immediately mounted in a liquid-helium cryostat and cooled to 1.4 K.

To perform fluorescence microscopy and fluorescence-excitation spectroscopy, the samples were illuminated with a continuous-wave tuneable titanium–sapphire (Ti:Sa) laser (3900S, Spectra Physics) pumped by a frequency-doubled continuous-wave neodynium-yttrium-vanadat (Nd:YVO_4) laser (Millennia Vs, Spectra Physics) using a home-built microscope that can be operated either in wide field or confocal mode. To obtain a well-defined variation of the wavelength of the Ti:Sa laser the intracavity birefringent filter has been rotated with a motorized micrometre screw. For calibration purposes, a wavemeter has been used and an accuracy as well as a reproducibility of $1\,\mathrm{cm^{-1}}$ for the laser frequency has been verified.

A fluorescence-excitation spectrum of an individual light-harvesting complex was obtained in two steps. First a $40 \times 40\,\mu\mathrm{m}^2$ wide-field image of the sample was taken by exciting the sample through a simple planoconvex lens with a large focal length ($f = 140$ mm; figure 2(a)). The excitation wavelength was chosen to coincide with an absorption maximum of the complexes (800 nm), whereas the emitted light was collected by a single aspheric lens ($f = 1.45$ mm, NA = 0.55) mounted inside the cryostat immersed in liquid helium and focused onto a back-illuminated CCD camera (512 SB, Princeton Instruments) after passing suitable

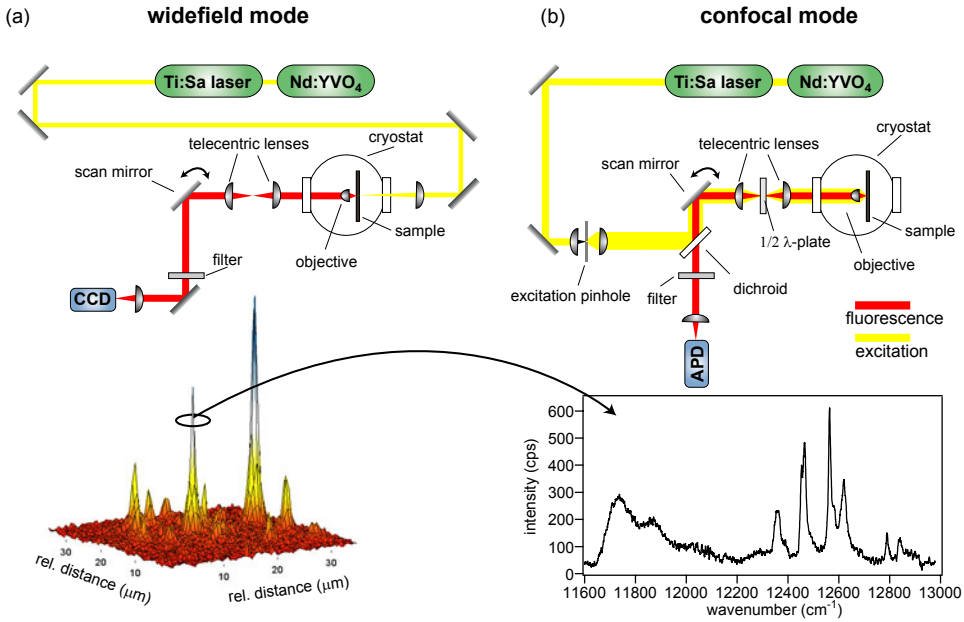

Figure 2. Experimental set-up for low-temperature single-molecule fluorescence microscopy. (a) Top: schematic sketch of the widefield arrangement of the microscope. Bottom: three-dimensional representation of a fluorescence image of about $40 \times 40\ \mu m^2$. Each peak corresponds to the diffraction-limited image of an individual LH2 complex. (b) Top: schematic sketch of the confocal arrangement of the microscope. Bottom: fluorescence-excitation spectrum of an individual LH2 complex from *Rs. molischianum*. See text for more details.

bandpass filters ($\Delta\lambda \approx 20$ nm) which blocked the residual laser light. The three-dimensional representation of the fluorescence—as depicted in the lower panel of figure 2(a)—shows several peaks each corresponding to the diffraction-limited image of an individual LH2 complex. The lateral resolution of the microscope was determined to 1 μm which is in agreement with the value expected theoretically. In the next step, a spatially well-isolated complex was selected from the wide-field image and a fluorescence-excitation spectrum of this complex was obtained by switching to the confocal mode of the set-up (figure 2(b)). In this mode, the excitation light was passed through an excitation pinhole and focused onto the sample by the objective lens inside the cryostat creating a diffraction-limited excitation volume of less than 1 μm^3. This volume was made to coincide with the complex by tilting the direction of the excitation beam with a scan mirror. A pair of telecentric lenses ensured a precise and well-controlled displacement of the focus on the sample while maintaining alignment with the confocal aperture.

The fluorescence was collected by the same objective lens and focused onto a single-photon-counting avalanche photodiode (APD) (SPCM-AQR-16, EG&G), which also fulfilled the role of the detection pinhole. Instead of obtaining a spectrum by slowly scanning the laser once, spectra were recorded in rapid succession by scanning repetitively through the spectral range of interest and storing the different traces separately. Thereby, light-induced fluctuations of the fluorescence intensity on a time scale of seconds could be diminished [23] and information about the spectral dynamics could be obtained. With a scan speed of the laser of 3 nm s^{-1} ($\approx 50\ cm^{-1}\ s^{-1}$) and an acquisition time of 10 ms per data point, this yields a nominal resolution

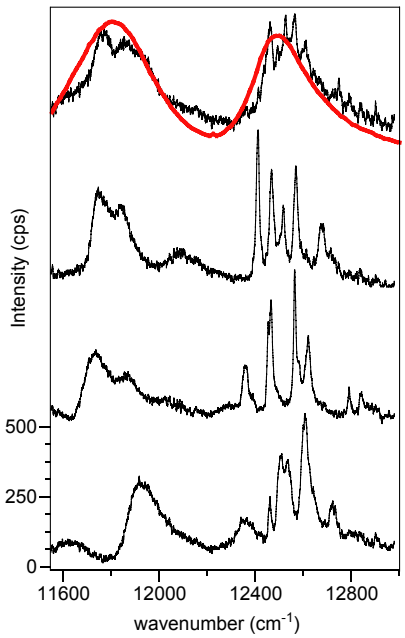

Figure 3. Fluorescence-excitation spectra of the B800 band of LH2 complexes from *Rs. molischianum*. The top traces show the comparison between a room-temperature ensemble spectrum (red) and the sum of 24 spectra recorded from individual complexes (black). The lower three traces display spectra from single LH2 complexes recorded at 1.4 K with an excitation intensity of 10 W cm^{-2}. Each individual spectrum has been averaged over all possible excitation polarizations. The vertical scale is valid for the lowest trace; all other traces were offset for clarity.

of 0.5 cm^{-1} ensuring that the spectral resolution is limited by the spectral bandwidth of the laser (1 cm^{-1}). The confocal-detection mode features a superior background suppression which allowed to record fluorescence-excitation spectra with high signal-to-noise ratios as shown, for example in the lower panel of figure 2(b).

To examine the polarization dependence of the spectra, a $\lambda/2$ plate was put in the confocal excitation path. It can be rotated in steps of 0.9° between two successive scans changing the angle of the polarization of the excitation light with twice this value. Owing to noise limitations of the signal, the orientation of the transition-dipole moment of an absorption could be determined within 5° accuracy with respect to the laboratory frame.

3. Experimental results

In figure 3, we compare several fluorescence-excitation spectra of LH2 from *Rs. molischianum*. The red line in the upper trace shows the spectrum obtained from a large ensemble. For illustration, we show as well the sum of 24 spectra obtained from individual complexes by the solid line. Both spectra are in good agreement and consist of two broad bands at 12 500 cm^{-1} (800 nm) and at 11 800 cm^{-1} ($\approx$ 850 nm), each featuring a linewidth of about 300 cm^{-1} (FWHM). Spectroscopy of individual LH2 complexes reveals a striking difference between the two absorption bands.

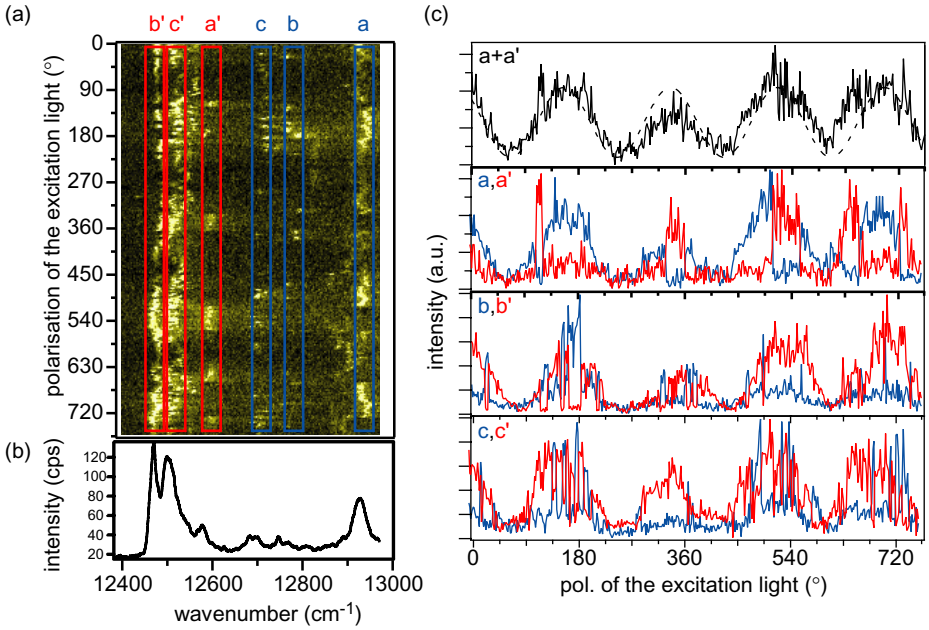

Figure 4. (a) Two-dimensional representation of 425 fluorescence-excitation spectra from the B800 band of an individual LH2 complex (complex 1). The spectra have been recorded consecutively at a scan speed of 50 cm^{-1} s^{-1} at an excitation intensity of 15 W cm^{-2}. The fluorescence intensity is indicated by the colour scale. Between two successive scans, the polarization of the excitation light has been rotated by 1.8°. The horizontal axis corresponds to the laser-excitation energy and the vertical axis to polarization. (b) Average of all 425 fluorescence-excitation spectra. (c) The traces in the lower three panels show the intensity of the three absorption pairs (a-a′, b-b′ and c-c′) indicated by the boxes in (a) as a function of the polarization. The trace in the topmost panel shows the sum of the traces of line pair a-a′ and a fitted $\cos^2$ function (dashed line).

The B850 is dominated by a few broad bands which reflect the exciton character of the involved electronic excitations, whereas the B800 band consists of several narrow lines which correspond to excitations that are (mainly) localized on individual BChl *a* molecules [20, 21].

To follow the spectral dynamics of the B800 absorptions, we swept the laser consecutively through the B800 spectral region and rotated the polarization of the incident laser light by a $\lambda/2$ plate by 1.8° between two successive scans. The individual fluorescence-excitation spectra were stacked on top of each other as shown in figure 4(a) (complex 1), where the horizontal axis corresponds to excitation energy, the vertical axis to the polarization angle of the excitation light with respect to the laboratory frame and the colour code to the fluorescence intensity. The fluorescence-excitation spectrum that results when the whole sequence of spectra is averaged is shown in figure 4(b). Interestingly, the individual B800 absorptions featured strong intensity fluctuations that cannot exclusively be explained by the rotation of the polarization of the exciting laser. As an example, the fluorescence intensities of the two absorptions at 12 928 and 12 587 cm^{-1}, labelled 'a' and 'a′', are plotted as a function of the polarization of the excitation light in the one but topmost panel in figure 4(c) in blue and red respectively. Comparison of

Table 1. For each absorption line observed for complex 1 (figure 4) the following parameters are listed: the label of the absorption line according to figure 4, the spectral position ν, the spectral distance $\Delta\nu$ between the two anti-correlated line positions, the rate k at which the absorption switches on average to the anti-correlated line position, the average spectral change of the peak position $\Delta\nu_{\mathrm{peak}}$ between two successive scans, and the accumulated linewidth observed in the averaged spectrum $\mathrm{FWHM}_{\mathrm{avg}}$ (figure 4b).

Absorption	ν (cm^{-1})	$\Delta\nu$ (cm^{-1})	k (s^{-1})	$\Delta\nu_{\mathrm{peak}}$/scan ($\mathrm{cm}^{-1}$)	$\mathrm{FWHM}_{\mathrm{avg}}$ (cm^{-1})
a	12 928	341	0.0005	5.3	39.1
a′	12 587		0.002	5.4	21.1
b	12 754	270	0.006	6.8	11.2
b′	12 484		0.001	3.9	28.5
c	12 698	180	0.008	6	70.3
c′	12 518		0.001	3.6	46.7

the two traces yields that the intensity fluctuations of the spectral features 'a' and 'a′' are anti-correlated. More evidence for this assumption is obtained by inspecting the sum of the two polarization traces, which is shown in the topmost panel in figure 4(c). It can be fitted by a $\cos^2$ function (dashed line) in agreement with the expectation for a linear absorber. Similarly, the absorptions b-b′ and c-c′ show an anti-correlated time dependence as well (one but lowest and lowest panel in figure 4(c)). However, the spectral changes between aa′, bb′, and cc′ occur mutually independent of each other. The width of the reversible spectral jumps lies between 180 and 341 cm^{-1}, and the rates at which these spectral fluctuations occur are in general very small and vary between 0.0005 and 0.008 s^{-1}. Interestingly, for none of the absorptions, the change in resonance frequency is accompanied by a significant change of the orientation of the transition-dipole moment. In addition to the large spectral changes described above, each of the absorptions shows excursions in frequency space of about 5 cm^{-1} between two successive laser scans. From the scan speed of the laser, we can obtain a lower boundary of 0.03 s^{-1} for the rate of those fluctuations. Since the homogeneous linewidth of the B800 absorptions amounts to 2–10 cm^{-1} [22, 29], the observed linewidth of 10–70 cm^{-1} results mainly from the accumulation of many small spectral shifts during the experiment of 230 min. Details are summarized in table 1.

For other LH2 complexes, spectral patterns could be found that showed a reversible switching of the complete B800 spectra between two distinct realizations. An example is shown in figure 5 (complex 2). As before, the spectra were recorded sequentially. The horizontal axis corresponds to excitation energy, the vertical axis to time and the colour code to the fluorescence intensity. The fluorescence-excitation spectrum that results when the whole sequence of spectra is averaged is shown in figure 5(b). Visual inspection of the time-resolved representation of the spectra leads to the conjecture that some of the absorptions show large spectral jumps between a limited number of spectral positions. This becomes even more evident if only parts of the total sequence of fluorescence-excitation spectra are displayed. Each spectrum shown in figure 5(c) results from the average of the individual traces over the time interval boxed in part (a) of the

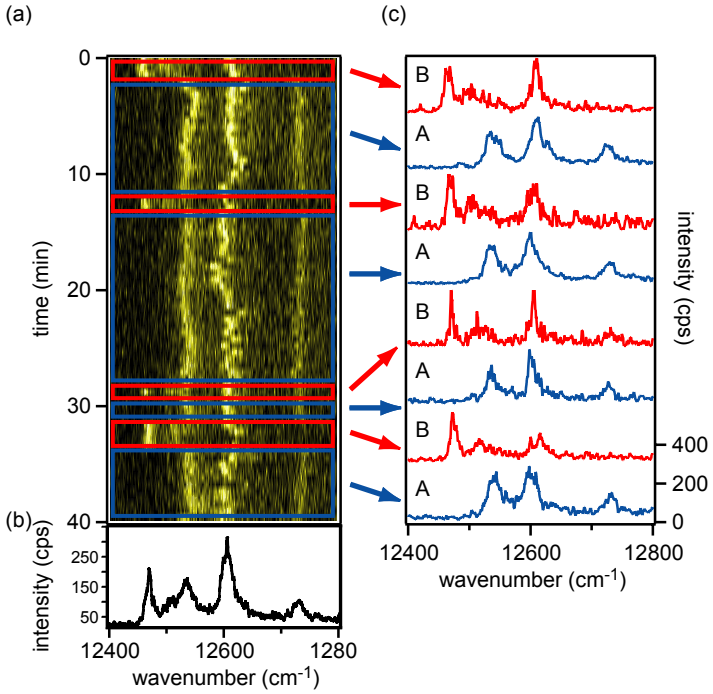

Figure 5. (a) Two-dimensional representation of 70 fluorescence-excitation spectra from the B800 band of an individual LH2 complex (complex 2). The spectra have been recorded consecutively at a scan speed of $50\,\mathrm{cm^{-1}\,s^{-1}}$ at an excitation intensity of $10\,\mathrm{W\,cm^{-2}}$. The fluorescence intensity is indicated by the colour scale. The horizontal axis corresponds to the laser-excitation energy and the vertical axis to time. (b) Average of all 70 fluorescence-excitation spectra. (c) Fluorescence-excitation spectra that result when the individual traces are averaged over the time windows boxed in (a). The vertical scale is valid for the lowest trace; all other traces were offset for clarity.

figure. It is clearly evident that for this particular complex the B800 spectrum corresponds to the time average of two distinct spectra, termed A and B hereafter. The conversion between the two spectra occurs as a reversible sudden spectral jump which is recurrent on a time scale of minutes. Another example for a LH2 complex that showed this phenomenon is shown in figure 6 (complex 3) as well as in an animated movie in the multimedia enhancement accompanying the paper. The set-up of figure 6 is similar to that of figure 5.

Since we do not observe spectral jumps of individual absorption lines as for complex 1, it is impossible to assign the spectral shifts directly. To find a quantitative measure for the observed spectral variations, we introduce the spectral mean $\bar{\nu}$ and the standard deviation σ_ν of the intensity distribution of the fluorescence-excitation spectra by

$$\bar{\nu} = \frac{\sum_i I(i)\nu(i)}{\sum_i I(i)}$$

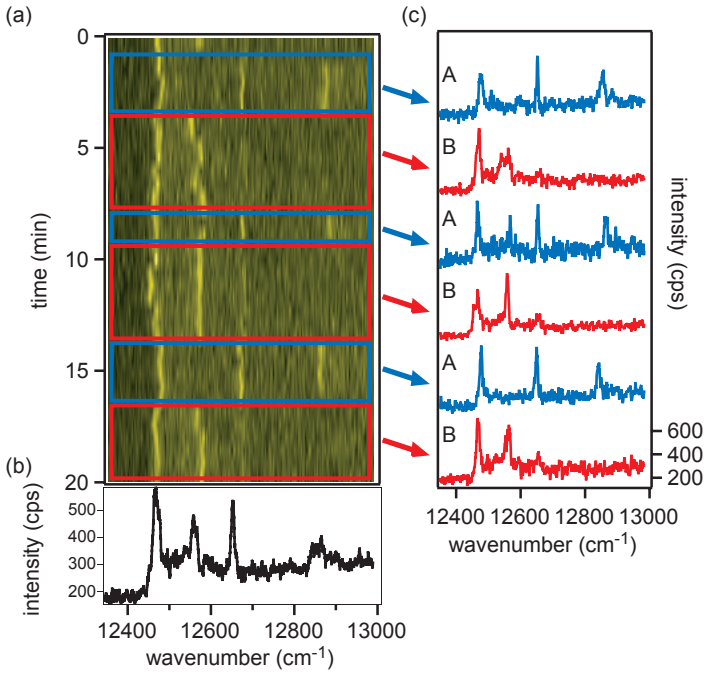

Figure 6. (a) Two-dimensional representation of 35 fluorescence-excitation spectra from the B800 band of an individual LH2 complex (complex 3). The spectra have been recorded consecutively at a scan speed of 50 $\mathrm{cm}^{-1}\,\mathrm{s}^{-1}$ at an excitation intensity of 60 $\mathrm{W\,cm}^{-2}$. The fluorescence intensity is indicated by the colour scale. The horizontal axis corresponds to the laser-excitation energy and the vertical axis to time. (b) Average of all 35 fluorescence-excitation spectra. (c) Fluorescence-excitation spectra that result when the individual traces are averaged over the time windows boxed in (a). The vertical scale is valid for the lowest trace; all other traces were offset for clarity.

and

$$\sigma_\nu = [\overline{\nu^2} - \overline{\nu}^2]^{1/2},$$

where

$$\overline{\nu^2} = \frac{\sum_i I(i)[\nu(i)]^2}{\sum_i I(i)}.$$

$I(i)$ corresponds to the fluorescence intensity at datapoint i, $\nu(i)$ refers to the spectral position that corresponds to datapoint i, and the sum runs over all datapoints of the spectrum. Accordingly, we characterize the distinct spectra A and B observed for the complexes 2 and 3 by the positions of the absorptions (ν_A, ν_B), their spectral means $(\bar{\nu}_A, \bar{\nu}_B)$, their standard deviations (σ_A, σ_B) and the rates at which the spectral changes occur $(k_{A\to B}, k_{B\to A})$.

For complex 2, the spectral mean changes by 61 cm^{-1} between the two spectral realizations, whereas the standard deviation remains nearly unchanged at about 90 cm^{-1}. The mean observation times for the spectra are $\tau_A = 500\,\mathrm{s}$ $(k_{A\to B} = 0.002\,\mathrm{s}^{-1})$ and $\tau_B = 83\,\mathrm{s}$

Table 2. Spectral features for the A- and B-type spectra of complexes 2 and 3 (figures 5 and 6). The spectral position ν of the absorption line is given together with the FWHM. The spectral mean is indicated by $\bar{\nu}$ and the standard deviation σ is given for the overall B800 spectrum, and k gives the average rate for the spectral change from A→B or B→A, respectively.

A					B				
ν_A (cm^{-1})	$FWHM_A$ (cm^{-1})	$\bar{\nu}_A$ (cm^{-1})	σ_A (cm^{-1})	$k_{A\to B}$ (s^{-1})	ν_B (cm^{-1})	$FWHM_B$ (cm^{-1})	$\bar{\nu}_B$ (cm^{-1})	σ_B (cm^{-1})	$k_{B\to A}$ (s^{-1})
Complex 2, figure 5									
12 733	28				12 614	32			
12 609	35	12 639	91	0.002	12 522	33	12 578	93	0.012
12 541	21				12 477	10			
Complex 3, figure 6									
12 850	37				12 654	12			
12 651	7	12 748	163	0.009	12 557	20	12 541	63	0.004
12 447	11				12 468	12			

($k_{B\to A} = 0.012\,s^{-1}$), respectively. A summary of these data is given in table 2. For complex 3, the spectral mean $\bar{\nu}$ changes between the A- and B-type spectra by 207 cm^{-1}. In contrast to complex 2, the standard deviation decreases from 163 to 63 cm^{-1}. The A-type spectrum can be observed, on average, for 110 s ($k_{A\to B} = 0.009\,s^{-1}$) before it switches to the B-type spectrum which remains, on average, for 250 s ($k_{B\to A} = 0.004\,s^{-1}$).

4. Discussion

The spectroscopic properties of the chromophores embedded in the photosynthetic complexes are determined to a large extent by their mutual spatial arrangement and their interaction with the local environment. However, a protein is not a rigid structure. It consists of a linear chain of amino acids folded into secondary and tertiary structure elements. Owing to the relatively weak interactions that stabilize the three-dimensional protein structure the lowest energy state of a protein is not unique. The potential energy hypersurface has $3N$ dimensions, where N is the number of atoms (typically >1000) in the protein, and features a multitude of minima, maxima and saddle points. Commonly, a description in terms of a rugged energy landscape is appropriate where each minimum represents a different conformational substate (CS) of the protein. To describe protein dynamics and function a model has been put forward by Frauenfelder and others [30]–[32], which proposes an arrangement of the protein energy landscape in hierarchical tiers. On each level of the hierarchy, the CS are characterized by an average energy barrier between the CS that decreases with descending hierarchy. A consequence of this idea is that structural fluctuations of a protein become hierarchically organized as well, featuring characteristic rate distributions in different tiers. Supporting evidence for this concept has been obtained from experimental work on myoglobin [30], [33]–[37].

In the context of a rugged protein energy landscape that is organized in tiers, the spectral dynamics observed in the B800 spectra can be interpreted straightforwardly. Since conformational changes of the protein correspond to rearrangements of its atoms, the embedded chromophores are subjected to fluctuations in the electrostatic interactions. The general idea is that the conformational changes are induced by optical excitation of the pigment. Given the low fluorescence quantum yield of LH2 of about 10% [38], a significant fraction of the average absorbed energy is dissipated by radiationless decay and excites nuclear motions of the protein matrix (phonons). If the system is prior to the optical excitation in an initial CS there is finite probability that it will end up in a different CS after the excitation and subsequent relaxation to thermal equilibrium. The dissipated energy exceeds the thermal energy significantly and the space of conformational substates that can be probed is not restricted to the part of the energy landscape that is thermally accessible.

Consequently, we attribute the observed spectral fluctuations to reflect modulations of the local interactions of the pigments. The huge spectral shifts observed for complex 1 are thought to result from conformational changes of the protein between two CS that are separated by a significant barrier height. The smaller spectral shifts are interpreted to result from conformational changes of the protein between several CS at the next lower tier that are separated by a minor barrier height. During the experiment, the distribution of CS on this tier is sampled and causes the observed linewidth of several 10 cm^{-1}. This interpretation is consistent with the observation of two distinct time scales for the spectral variations—huge spectral changes occur at slow rates, small spectral changes occur at faster rates. Since the relevant pigment–protein interactions are strongly distance-dependent, it is reasonable to assume that the conformational changes occur in the local environment of the chromophores.

To understand the observations in connection with complexes 2 and 3, one has to consider that the excitations of the B800 BChl *a* molecules can be treated only in first approximation as being localized on individual molecules. To avoid confusion, we distinguish between Δ which refers to the width of the distribution of site energies of the ensemble of pigments and δ, which refers to the actual difference in site energy between two individual, adjacent BChl *a* molecules. Previously, we have shown [21] that the ratio of the intermolecular interaction strength, V, and the energy mismatch in site energy, δ, between adjacent BChl *a* molecules is subjected to a distribution. The actual value of V/δ varies between different LH2 complexes and even between different B800 BChl *a* molecules within the same complex. The values that we obtained cover typically a range of $V/\delta \approx 0.3$–2.5. Therefore, it is very probable that for some LH2 complexes the B800 excitations are slightly delocalized over 2–3 monomer units. This is corroborated by the observation of about 4–6 absorptions in the B800 spectra from individual LH2 complexes [21, 24] rather than 8 absorptions (or 9 for LH2 from *Rhodopseudomonas acidophila*) as should be observable for strictly localized excitations.

However, both the difference in site energy, δ, of two pigments and the intermolecular interaction strength, V, depend critically on the mutual orientation and the distance of the pigments. Any change in the protein backbone induces a variation of the local V/δ ratio, which is manifested as a change of the optical spectrum. To illustrate this interpretation, we show in figure 7 a schematic sketch of a part of the B800 ring. We emphasize that the figure has only illustrative character and that we cannot determine the actual distribution of the excitation energy in the B800 assembly. We denote the coupling strength between adjacent molecules 'i' and 'j' by V_{ij}/δ_{ij} and it is realistic to assume that its actual value is different for each pair of molecules. In the top part of figure 7, we show an arbitrary situation, termed 'A', where

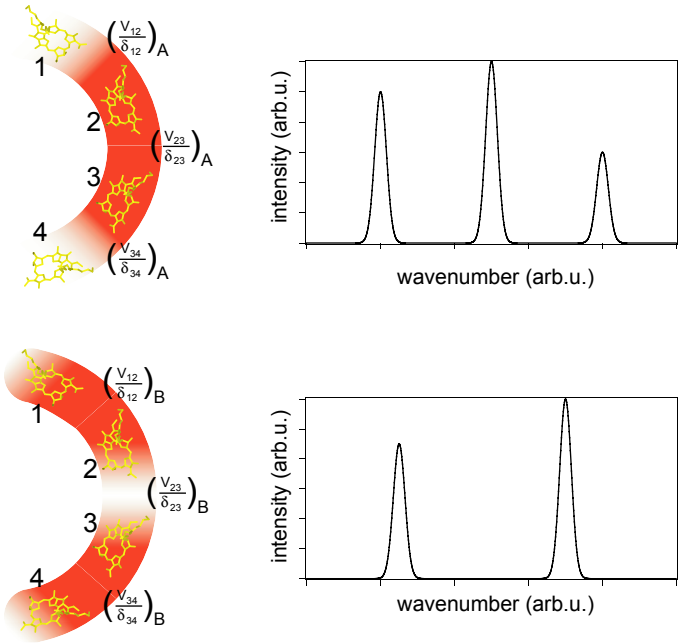

Figure 7. Schematic sketch to illustrate the interpretation of the experimental results in connection with figures 5 and 6. On the left-hand side, a part of the B800 assembly is shown. The local intermolecular coupling between the individual B800 molecules 'i' and 'j' is indicated by V_{ij}/δ_{ij}. The right-hand side of the figure shows two (arbitrary) fluorescence-excitation spectra for two different sets of coupling parameters, denoted by the subscripts A and B.

the excitation is localized on molecules 1 and 4 and delocalized between molecules 2 and 3. In the lower part of figure 7, we show an arbitrary situation, termed 'B', where the distribution of intermolecular couplings has changed such that the excitation becomes delocalized between molecules 1 and 2 as well as between molecules 3 and 4. Despite the arbitrarily chosen examples for the illustration, it is doubtless that such kind of variations in the electronic couplings result in changes of the optical spectrum.

Support for the conjecture that the observed spectral fluctuations are caused by conformational changes of the protein-binding pocket of the chromophore comes from several investigations. From theoretical work, it is known that the site energy of a BChl *a* molecule is very sensitive to perturbations of the π-conjugation of the bacteriochlorin macrocycle which can lead to shifts of up to 500 cm^{-1} for the optical transition energy [39]. Site-directed mutagenesis on LH2 from *Rhodobacter sphaeroides* has shown that fluctuations in the strength of a hydrogen bond that is formed between a residuum of the protein backbone and the C_2 acetyl group of the BChl *a* molecule lead to spectral shifts of 100–200 cm^{-1} of the B800 ensemble absorption [40, 41]. By spectral hole-burning spectroscopy on LH2 from *Rhodopseudomonas acidophila*, it has been found that relative distance changes of $\Delta R/R \approx 10^{-4}$–$10^{-2}$ are already sufficient to result in spectral shifts of 1–100 cm^{-1} for the B800 absorptions [42].

The various approaches agree in the conclusion that structural changes within the binding pocket of the chromophore result in spectral variations of several 100 cm^{-1} for the B800 absorptions which is consistent with our work. Many of the complexes that we have studied

featured a more complex temporal development of the spectra due to simultaneous spectral jumps of multiple chromophores. Only for a small fraction of LH2 complexes we found either the simple 'two-state jumps' as for complex 1 or the 'spectral switching' behaviour as for complexes 2 and 3. It is one of the intriguing features of single-molecule spectroscopy to isolate such key processes which might become essential for the development of a more general model of protein dynamics.

Acknowledgments

This work is financially supported by the Volkswagen Foundation within the framework of the priority area 'Physics, Chemistry and Biology with Single Molecules'. We thank Cornelia Münke for her technical assistance and J Friedrich for fruitful discussions.

References

[1] Moerner W E and Kador L 1989 *Phys. Rev. Lett.* **62** 2535–2538
[2] Orrit M and Bernard J 1990 *Phys. Rev. Lett.* **65** 2716–2719
[3] Strick T, Allemand J-F, Croquette V and Bensimon D 2000 *Prog. Biophys. Mol. Biol.* **74** 115–140
[4] Harms G S, Cognet L, Lommerse P H M, Blab G A and Schmidt Th 2001 *Biophys. J.* **80** 2396–2408
[5] Hugel T, Holland N B, Cattani A, Moroder L, Seitz M and Gaub H E 2002 *Science* **296** 1103–1106
[6] Sauer M, Angerer B, Ankenbauer W, Földes-Papp Z, Göbel F, Han K-T, Rigler R, Schulz A, Wolfrum J and Zander C 2001 *J. Biotechnol.* **86** 181–201
[7] Ali M Y, Uemura S, Adachi K, Itoh H, Kinosita K Jr and Ishiwata S 2002 *Nat. Struct. Biol.* **9** 464–467
[8] Yasuda R, Masaike T, Adachi K, Noji H, Itoh H and Kinosita K Jr 2003 *Proc. Natl Acad. Sci. USA* **100** 9314–9316
[9] Lounis B and Moerner W E 2000 *Nature* **407** 491–493
[10] Tamarat P, Maali A, Lounis B and Orrit M 2000 *J. Phys. Chem.* A **104** 1–16
[11] Orrit M 2002 *J. Chem. Phys.* **117** 10938–10946
[12] Moerner W E 2002 *J. Phys. Chem.* B **106** 910–927
[13] Köhler J, Disselhorst J A J M, Donckers M C J M, Groenen E J J, Schmidt J and Moerner W E 1993 *Nature* **363** 242–244
[14] Wrachtrup J, von Borczyskowski C, Bernard J, Orrit M and Brown R 1993 *Nature* **363** 244–245
[15] McDermott G, Prince S M, Freer A A, Hawthornthwaite-Lawless A M, Papiz M Z, Cogdell R J and Isaacs N W 1995 *Nature* **374** 517–521
[16] Koepke J, Hu X, Muenke C, Schulten K and Michel H 1996 *Structure* **4** 581–597
[17] McLuskey K, Prince S M, Cogdell R J and Isaacs N W 2001 *Biochemistry* **40** 8783–8789
[18] van Amerongen H, Valkunas L and van Grondelle R 2000 *Photosynthetic Excitons* (Singapore: World Scientific)
[19] van Oijen A M, Ketelaars M, Köhler J, Aartsma T J and Schmidt J 1999 *Science* **285** 400–402
[20] Ketelaars M, van Oijen A M, Matsushita M, Köhler J, Schmidt J and Aartsma T J 2001 *Biophys. J.* **80** 1591–1603
[21] Hofmann C, Ketelaars M, Matsushita M, Michel H, Aartsma T J and Köhler J 2003 *Phys. Rev. Lett.* **90** 013004
[22] van Oijen A M, Ketelaars M, Köhler J, Aartsma T J and Schmidt J 2000 *Biophys. J.* **78** 1570–1577
[23] van Oijen A M, Ketelaars M, Köhler J, Aartsma T J and Schmidt J 1998 *J. Phys. Chem.* B **102** 9363–9366
[24] van Oijen A M, Ketelaars M, Köhler J, Aartsma T J and Schmidt J 1999 *Chem. Phys.* **247** 53–60

[25] Matsushita M, Ketelaars M, van Oijen A M, Köhler J, Aartsma T J and Schmidt J 2001 *Biophys. J.* **80** 1604–1614
[26] Ketelaars M, Hofmann C, Köhler J, Howard T D, Cogdell R J, Schmidt J and Aartsma T J 2002 *Biophys. J.* **83** 1701–1715
[27] Hofmann C, Francia F, Venturoli G, Oesterhelt D and Köhler J 2003 *FEBS Lett.* **546** 345–348
[28] Germeroth L, Lottspeich F, Robert B and Michel H 1993 *Biochemistry* **32** 5615–5621
[29] de Caro C A, Visschers R W, van Grondelle R and Völker S 1994 *J. Phys. Chem.* **98** 10584–10590
[30] Frauenfelder H, Sligar S G and Wolynes P G 1991 *Science* **254** 1598–1603
[31] Nienhaus G U and Young R D 1996 *Encyclopedia of Applied Physics* vol 15, pp 163–184
[32] Frauenfelder H, Nienhaus G U and Young R D 1994 *Disorder Effects on Relaxational Processes*, ed R Richert (Berlin: Springer) pp 591–614
[33] Frauenfelder H and McMahon B H 2001 *Single Molecule Spectroscopy (Nobel Conference Lectures)*, eds R Rigler, M Orrit and T Basché (Berlin: Springer) pp 257–276
[34] Frauenfelder H, McMahon B H, Austin R H, Chu K and Groves J T 2001 *Proc. Natl Acad. Sci. USA* **98** 2370–2374
[35] Leeson D T, Wiersma D A, Fritsch K and Friedrich J 1997 *J. Phys. Chem.* B **101** 6331–6340
[36] Fritsch K, Friedrich J, Parak F and Skinner J L 1996 *Proc. Natl Acad. Sci. USA* **93** 15141–15145
[37] Parak F and Nienhaus G U 2002 *ChemPhysChem.* **3** 249–254
[38] Monshouwer R, Abrahamsson M, van Mourik F and van Grondelle R 1997 *J. Phys. Chem.* B **101** 7241–7248
[39] Gudowska-Novak E, Newton M D and Fajer J 1990 *J. Phys. Chem.* **94** 5795–5801
[40] Gall A, Fowler G J S, Hunter C N and Robert B 1997 *Biochemistry* **36** 16282–16287
[41] Fowler G J S, Visschers R W, Grief G G, van Grondelle R and Hunter C N 1992 *Nature* **355** 848–850
[42] Zazubovich V, Jankowiak R and Small G J 2002 *J. Phys. Chem.* B **106** 6802–6814